Applied Energy 215 (2018) 543–555

Contents lists available at ScienceDirect

Applied Energy

journal homepage: www.elsevier.com/locate/apenergy

Experimental study of a small scale organic Rankine cycle waste heat recovery system for a heavy duty diesel engine with focus on the radial inflow turbine expander performance

Fuhaid Alshammari[a], Apostolos Pesyridis[a,b,*], Apostolos Karvountzis-Kontakiotis[a], Ben Franchetti[c], Yagos Pesmazoglou[c]

[a] Brunel University London, Department of Mechanical, Aerospace & Civil Engineering, CAPF – Centre of Advanced Powertrain and Fuels, Uxbridge UB8 3PH, United Kingdom
[b] Metapulsion Engineering Ltd, Northwood, London, United Kingdom
[c] Entropea Labs Ltd, London E8 1AB, United Kingdom

HIGHLIGHTS

- An advanced ORC system, tested on a 200 kW – class off-highway diesel engine.
- A radial ORC turbine expander with novel back-swept blading tested experimentally.
- A state-of-the-art molecularly-complex working fluid was tested.
- Integrated generator electrical system power and efficiency measured.
- Maximum 4.3% ORC system efficiency at 40% load on NRTC cycle at 1700 rpm (80 kW).

ARTICLE INFO

Keywords:
Organic Rankine cycle
Heavy duty diesel engine
Radial inflow turbine
Waste heat recovery

ABSTRACT

The purpose of this work is to experimentally evaluate the effect on fuel efficiency of a small scale organic Rankine cycle (ORC) as a waste heat recovery system (WHRS) in a heavy duty diesel engine that operates at steady state conditions. The WHRS consists of two operating loops, namely a thermal oil loop that extracts heat from the engine exhaust gases, and the working fluid loop which is the ORC system. The expansion machine of the ORC system is a radial inflow turbine with a novel back-swept blading that was designed from scratch and manufactured specifically for this WHR application. The engine test conditions include a partial engine load and speed operating point where various operating conditions of the ORC unit were tested and the maximum thermal efficiency of the ORC was defined close to 4.3%. Simultaneously, the maximum generated power was 6.3 kW at 20,000 rpm and pressure ratio of 5.9. The isentropic efficiency reached its peak of 35.2% at 20,000 rpm and 27% at 15,000 rpm. The experimental results were compared with the CFD results using the same off-design conditions, and the results were in good agreement with a maximum deviation of 1.15% in the total efficiency. Last but not least, the engine-WHRS energy balance is also discussed and presented.

1. Introduction

State of the art internal combustion engines (ICE) waste a substantial amount of fuel energy in the form of exhaust gases and engine coolant heat loss. Modern commercial road and off-road heavy-duty diesel engines present a maximum brake thermal efficiency value of approximately 45% at their optimum operating point [1], while gasoline engine maximum thermal efficiency is typically between 30% and 40% [2]. Engine wasted heat is not only a waste of fuel but also a matter of significant global warming and environmental pollution concerns. CO_2 emissions from the transportation sector have increased by 45% between 1990 and 2007, making this sector responsible for nearly one third of the world's CO_2 emissions. Therefore, manufacturers of ICEs are increasingly forced to look at the feasibility of adopting

* Corresponding author at: Brunel University London, Department of Mechanical, Aerospace & Civil Engineering, CAPF – Centre of Advanced Powertrain and Fuels, Uxbridge UB8 3PH, United Kingdom.
E-mail address: a.pesyridis@brunel.ac.uk (A. Pesyridis).
URL: http://www.brunel.ac.uk/people/apostolos-pesyridis (A. Pesyridis).

https://doi.org/10.1016/j.apenergy.2018.01.049
Received 17 October 2017; Received in revised form 26 December 2017; Accepted 19 January 2018
Available online 20 February 2018

Nomenclature

Variables

h	enthalpy [kJ/kg]
$\dot{m}$	mass flow rate [kg/s]
P	pressure [bar]
P_e	electrical power [kW]
W	power output [kW]

Subscripts

0	total thermodynamic properties
1–2	stations within the cycle
s	isentropic
to	thermal oil
w_f	working fluid

Greek letters

η	efficiency [%]
τ	torque [N.m]

Acronyms

ASIC	Application Specific Integrated Circuit
BSFC	brake specific fuel consumption
ICE	internal combustion engine
ORC	organic Rankine cycle
rms	root mean square
TC	turbo-compounding
WHR	waste heat recovery

technologies such as waste heat recovery systems in order to reduce fuel consumption and CO_2 emissions.

Waste heat recovery technologies depend upon tapping into main heat sources in ICEs such as exhaust gas, EGR and/or engine coolant to be recovered. One such technology in use is Turbo-Compounding (TC) either in its mechanical or electrical forms. Depending on the engine load, TC can reduce the average BSFC by 3–6% with the ability of further reduction of 6.5% with highly efficient TC configurations [3]. In addition, combination of TC and steam injection could result in reduction of BSFC by 6.0–11.2% over different speeds [4]. However, it is worth mentioning that the utilization of TC in ICEs is limited due to the high exhaust backpressure caused by such technology and eventually higher pumping losses [5]. Another significant waste heat recovery technology proposition is thermoelectric generation. Experimental studies have shown that fuel savings of 3.9 up to 4.7% could be achieved by using thermo-electric generation [6–8]. However, this technology is currently too expensive and faced with a longer development time [9]. In addition, it still presents very poor efficiency (typically less than 4%). Therefore, it is of essence to investigate a more efficient and cheaper technology.

Organic Rankine Cycles (ORCs) have become popular in re-using wasted heat since they operate efficiently and use relatively simple standard components. Moreover, ORCs can take indirect advantage of the heat rather than the direct exhaust gas supply thus allow a much higher degree of freedom in optimising the expander. Using ORCs in mobile applications is not a new idea. A first concept on a train had already been commercialized in the 1920s, taking advantage of the price difference between diesel and coal [10]. Unfortunately, this system quickly became uncompetitive because that difference stopped being profitable [11]. Later, several systems were developed, mostly for trucks or marine applications, and then this interest disappeared until the 2000s, when automotive manufacturers started being interested in that technology again [11] largely due to regulatory pressure. Patel and Doyle [12] built a prototype of an ORC that was used as a bottoming cycle in a Mack 676 diesel engine. The authors stated that at the peak power condition, 36 additional horsepower was produced resulting in a gain of 13% in power without additional fuel. Recently, wide theoretical investigations have been conducted on ORC applications in ICEs [13–21]. The results indicate that the BSFC improvements of up to 10% can be obtained. However, these theoretical studies usually neglect electro-mechanical losses along the turbo-generator power transmission route and heat transfer to the environment. Realistic expectations are limited to approximately 50% of the above BSFC figures [22].

Selection of the appropriate expansion machines is of great importance when utilizing ORC systems since these machines are responsible for power conversion and subsequent production usually by direct coupling to a generator [22–25]. In addition, the type of expansion machine has significant effects on the overall cycle performance, size and cost [26,27]. Expanders can be classified into two main groups, namely, positive displacement expanders (Screw, Scroll, Piston and Rotary Vane) and turbo-machines (Axial or Radial). The selection of the appropriate expander depends on the application. Moreover, other important factors should be considered when selecting expanders such as high isentropic efficiency, pressure ratio, power output, lubrication requirements, complexity, rotational speed, dynamic balance, reliability, cost, working temperatures and pressures, leakage, noise and safety [28,29]. Turbo-expanders are preferred when to convert the extracted power to electricity while reciprocating expanders, due to their flexibility of operation, are preferred when the extracted power is coupled directly to the crankshaft [30]. Moreover, displacement expanders could be used at low output powers due to the limitation of their rotational speed [31], whereas turbo-expanders operate at higher rotational speed and hence higher power. However, for waste heat recovery applications, scroll expanders and radial turbines are the most common solutions to be found in literature [32,33]. Since ORC efficiency increases at high pressure ratios, radial turbines appear more suitable for vehicular applications where mass flow rates are in the low-to-medium range and pressure ratios are in the medium-to-high range.

Nowadays, ORC systems as WHR technologies are gaining attention in both academic and industrial sectors. Several recent studies have investigated ORC technology and show promise in solar systems [34–38], biomass [39–44] and geothermal applications [45–48]. In recent years, studies concentrating on ICE applications have increased. Zhang et al. [49] evaluated the wasted heat in the engine exhaust, intake air, and coolant of a vehicular light-duty diesel engine. It is worth mentioning that the performance map of the light-duty diesel engine was created using an engine test bench while the study of the coupled system (engine + ORC) was conducted using a simulation study. The results of the simulation study showed that the ORC output power improved from 14% to 16% in the peak effective thermal efficiency region and from 38% to 43% in the small load region. Furukawa et al. [50] conducted an experimental test on the ORC that was used to recover the heat of the engine coolant with Hydro-fluoro-ether as the working fluid. The fuel consumption decreased by 7.5%. Recently, Wang et al. [51] conducted a recent study on recovering the wasted heat of the exhaust gas and coolant of a CNG machine using a supercritical-subcritical dual-loop organic Rankine cycle. R1233zd and R1234yf were used as the working fluids. The engine point with 600 N.m and 1600 rpm was selected as the case study since CNG engine usually operates at low to middle speed and torque for bus applications. Similar to Zhang et al. [51], the engine map was obtained experimentally while the results of the integrated system (engine + ORC) were obtained using the simulation study. The simulations showed that fuel efficiency could be improved by more than 8% in most of the engine's

operating regions. Other recent studies such as Shao et al. [52] and Pang el al. [53] conducted experimental studies using radial turbine and scroll expander, respectively, as the expansion machines. However, both studies used oil heaters as the heat sources. The results of [52] showed that a maximum thermal efficiency of 5.3% and turbine efficiency of 75.2% were achieved. The results of the other study [53] showed that a maximum net power 1.66 kW with an electrical efficiency of about 4.4% were obtained. Guillaume et al. [17] used exhaust gases of a truck diesel engine as the heat source for their ORC system. They used a radial inflow turbine as the expansion machine and two working fluids: R245fa and R1233zd. However, the employed turbine was developed mainly using components modified from truck turbocharger designs. Also, the heat wasted by the truck through the exhaust gases is simulated using an electric oil boiler coupled to the ORC loop. The maximum electric power and turbine efficiency were 2.8 kW (using R245fa) and 32% (using R1233zd), respectively. Yang et al. [54] presented a thermo-economic model of a dual-loop ORC system using the performance map of a six-cylinder CNG engine. The thermal efficiency of the dual loop ORC system was in the range of 8.97–10.19% over the whole operating range. More recently, Sellers [55] evaluated the benefits of ORC systems in harnessing the wasted heat in the jacket water of a 12 cylinder ship engine. The paper was more about the difficulties that the author faced during the installation of the system. The results showed that the largest kilowatt hour value of 78,001 was produced during the first voyage from Asia to the USA east coast. In the industry sector, a recent study through cooperation between AVL, FPT and Iveco [56] was published. The exhaust gas of a 4-stroke diesel engine was used as the heat source for the ORC system, axial piston expander was selected as the expansion machine. The tests were run on public roads. The results showed that the fuel consumption could be reduced by 2.5–3.4%. Honda [57,58] installed an ORC system on a hybrid vehicle with the vehicle running at constant speed and the thermal efficiency increased by 13.2% compared to the base vehicle. MAN [59] installed a Rankine cycle system on a marine 2-stroke diesel engine and claimed that a 10% efficiency improvement was achieved.

The brief literature survey in the previous paragraph indicates that these investigations were either performed using simulated engine data (academic sector) or expanders types other than radial turbine (industry sector). Although Guillaume et al. [17] used a radial inflow turbine in their study, the turbine was developed using components of truck turbochargers. Also, they applied an electric oil boiler as the heat source. The coupling of a custom-designed radial turbine (and generator) on-engine to explore ORC WHR system performance is an area in which little available literature exists. To allow a realistic appreciation of the ORC system's contribution to heavy-duty diesel engine, a coupling of ORC system with real engine is essential. In the present work, a test rig containing an ORC thermal oil loop was built around a heavy-duty diesel engine and was tested. The radial turbine in the current study was designed and manufactured specifically for this application considering the cycle operating conditions and the working fluid properties. From the engine point of view, part-load performance is seldom investigated in depth and this is where the focus of this study was. For this study, the engine was operated at 40% of its maximum power targeting a representative, mean operating condition. The exhaust gas of a heavy duty diesel engine was applied as the heat source for the thermal oil loop. Then, the oil exchanged heat with the ORC unit. Direct heat transfer from the exhaust gases to the organic fluid is often preferred in transport applications as it increases the heat transfer efficiency and reduces the weight of the WHR system. On contrast, the thermal oil loop requires an extra heat exchanger and pump which increases the cost and weight and reduces the system efficiency. One main advantage of the oil loop is that it eases the control of the thermodynamic conditions in the ORC circuit. In addition, the combination of ORC-thermal oil loop is beneficial in order to keep the thermal oil temperature in the evaporator stable. The measurements were all performed in steady state conditions. The results of both the ORC cycle and specific turbine are all presented in the following pages.

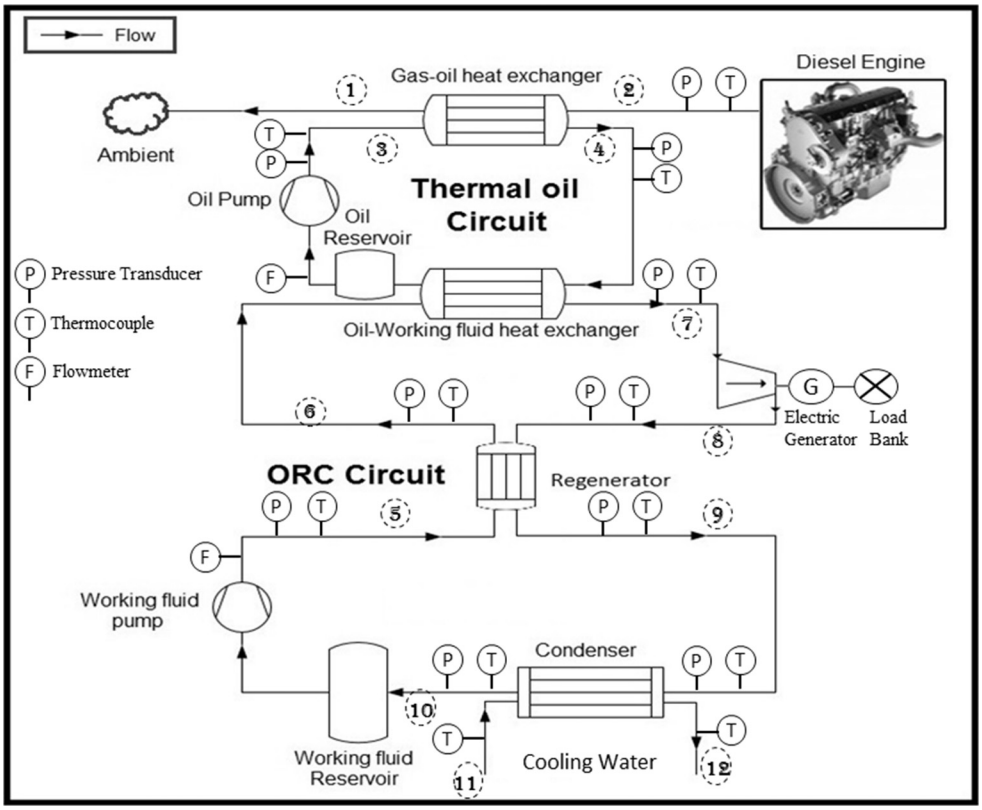

Fig. 1. Schematic representation of the test bench.

2. Working fluid selection

Selection of working fluid for an ORC system is of key importance for the cycle efficiency and network. It also represents the first step in the design of an ORC. In ORC systems, only working fluids with low Global Warming Potential (GWP) and Ozone Depletion Potential (ODP) should be utilized [60].

Among the hundreds of fluids available, it is necessary to select either non-flammable fluids or flammable fluids whose auto-ignition temperature is higher than that of the exhaust gasses leaving the ICE. For example, only a small subset of the Alkanes can be considered. In particular, the Alkanes that have a flammability limit that is higher than the heat source of the ORC in question. In order to come up with the optimum fluid for the current applications, the authors [61] proposed novel method for the selection of the proper working fluid for ORC-WHR systems based on a radial expander in which thermodynamic properties and evaporator heat transfer surface are taken into account. The detailed results of the proposed method can be found in [61]. The final screening was based on the effect of the organic fluids on the required components of the ORC, namely,

- The evaporator heat transfer surface needs to be minimized due to the space constraints since this component has to be fitted into the immediate surroundings of the ICE exhaust manifold.
- The Radial turbine rotational speed is known to affect the turbine efficiency (furthermore, excessive rotational speeds lead to manufacturing and operational problems). The expander/turbine is directly coupled to the Power Conversion Unit (PCU), which performs the mechanical-electrical power conversion, and the alternator would become much more expensive.
- The Back work ratio (BWR), i.e., the ratio between pump and turbine power, must be minimized to maximize the cycle net power output.
- The Turbine external diameter should fall within the dimensional constraints of the retrofitting capability of the technology.

Two fluids (Fluid A and R1233zde) were selected for further screening because they have zero toxicity, low GWP, maximum power output compared to others, and both are inflammable. The results were further expanded as shown in another work by the authors [5]. Overall, Fluid A was shown to produce lower back pressure at the evaporator exit. On the other hand, R1233zde presented very high turbine rotational speed which in turns had a negative effect on the electric generator cost. Moreover, according to 3M [62] that produced Fluid A, this fluid is an effective heat transfer fluid that can be utilized in applications such as ORC where non-flammability or environmental factors are a consideration. Last but not least, Fluid A, which unfortunately cannot be mentioned here for reasons of strict confidentiality, is generally more available in the market.

3. ORC thermodynamic definitions used in the experiment

This section presents the experimental set-up tested and the principal theoretical expressions used in the definition of the ORC system and expander performance. Fig. 1 presents the schematic layout of the ORC test rig. Thermal oil extracts the heat of the exhaust gas via the gas-oil heat exchanger (main heat exchanger). Using the working fluid pump, the working fluid is pumped at high pressure to the evaporator to extract the heat from the hot thermal oil. The superheated fluid then enters the turbine to rotate the turbine blades generating power output. The turbine is directly coupled to a high speed synchronous electric generator to convert the turbine mechanical power to electricity. In the test bench, a load bank is installed for the purpose of electric power dissipation. Since the working fluid leaving the evaporator is still hot, the fluid enters the recuperator to absorb the remaining heat. The warm working fluid then enters the condenser where it is condensed into liquid before entering the working fluid receiver tank and restarting the cycle.

Table 1 presents the principal thermodynamic equations of each component. Performance of the ORC system is measured using the definition of the thermal efficiency η_{ORC} as shown in Eq. (1). Thermal efficiency is defined as the ratio between the cycle work net and the heat extraction in the evaporator. W_{net} is the cycle power and it is the difference between the electrical power generated by the generator and the power consumed by the pumps (working fluid pump and thermal oil pump), Eq. (2).

$$\eta_{ORC} = \frac{W_{net}}{Q_{evap}} \tag{1}$$

$$W_{net} = P_e - (W_{pump,wf} + W_{pump,to}) \tag{2}$$

The performance of the turbine is measured using bulk properties for the total-to-total isentropic efficiency definition as shown in Eq. (3). $\boldsymbol{h_{08s}}$ is obtained using REFPROP [63] at $\{\boldsymbol{P_{08}}, \boldsymbol{s_{01}}\}$ as shown in the h-s diagram, Fig. 2. Another indicator of turbine performance is the turbine expansion power and it is defined using Eq. (4). Eq. (4) is a well know expression that combines the energy conservation and Euler equation. Euler equation can be defined in another form as shown in Eq. (5). According to Moustapha et al. [64], Euler equation can be combined with the velocity triangle to obtain Eq. (6), where a and b denotes the rotor inlet and exit, respectively.

$$\eta_{tt} = \frac{h_{07} - h_{08}}{h_{07} - h_{08s}} \tag{3}$$

$$W_{out} = \dot{m}\Delta h_{act} = \tau\omega \tag{4}$$

$$W_{out} = \dot{m}(U_a C_{\theta a} - U_b C_{\theta b}) \tag{5}$$

$$W_{out} = 0.5[(U_a^2 - U_b^2) - (W_a^2 - W_b^2) + (C_a^2 - C_b^2)] \tag{6}$$

4. Experimental apparatus

The test rig consists of two main components: the heavy duty diesel engine (Fig. 3) and the ORC skid (Fig. 4).

Table 1
Thermodynamic equations defining the operation of each component of the ORC.

Component	Equation	Equation #	Comments
Evaporator	$Q_{evap} = \dot{m}_{wf}(h_7 - h_6)$	(7)	Q_{evap} is the heat transfer in the evaporator in kW. h_6 and h_7 are enthalpies in kJ/kg at inlet and exit of the evaporator. $\dot{m}_{wf}$ is the mass flow rate of the working fluid
Turbine	$W_{turb} = \dot{m}_{wf}(h_7 - h_8)$	(8)	W_{turb} is the turbine power output in kW
Recuperator	$Q_{recup} = (h_6 - h_5) = (h_8 - h_9)$	(9)	Q_{recup} is the heat transfer in the recuperator in kW
Condenser	$Q_{cond} = \dot{m}_{wf}(h_9 - h_{10})$	(10)	Q_{cond} is the heat transfer in the condenser in kW
Pump	$W_{pump} = \dot{m}_{wf}(h_5 - h_{13})$	(11)	W_{pump} is the turbine power output in kW

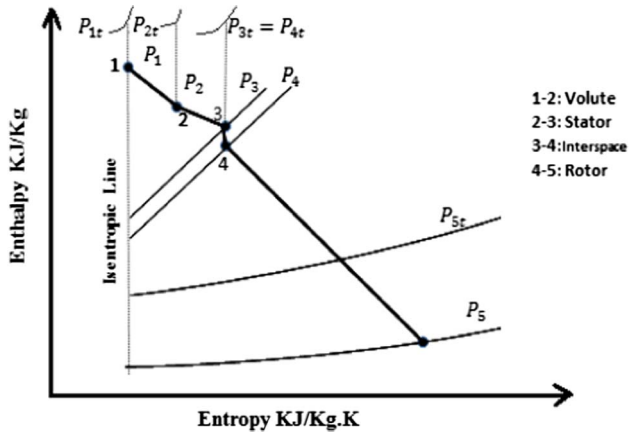

Fig. 2. Enthalpy-entropy diagram through the turbine stage [65].

4.1. Description of the heavy duty diesel engine

The heavy duty diesel engine utilized in the test is a 7.25ℓ Yuchai engine. It is a turbocharged, direct injection engine and fulfils the EURO III regulatory requirements. The detailed characteristics of the heavy duty diesel engine are presented in Table 2. The engine capacity is considered sufficient to apply a waste heat recovery system to, due to the high exhaust flow enthalpy available.

The engine exhaust heat map of this heavy duty diesel engine is illustrated at Fig. 5. It is observed that the maximum exhaust energy is wasted at maximum power conditions, which was also considered as the design point of this ORC unit, in order to maximize the ORC system power output. However in transient automotive applications the ORC system rarely operates at the design conditions. In this study, the presented tested off-design conditions of the ORC system are at 40% (81 kW) of the maximum engine power, as presented in Fig. 5. This operating point represents an average steady state operation between high and low engine load and speed of the non-road transient cycle (NRTC) test protocol. NRTC is a legislative driving cycle developed by US EPA in collaboration with EU and is utilized worldwide for type approval of non-road engines. The normalized engine speed and torque profile are also presented in Fig. 5.

4.2. ORC installation

This section presents a brief description of each component of the ORC system. Fig. 4 illustrates the installation which was tested in the powertrain test facility at Brunel University London.

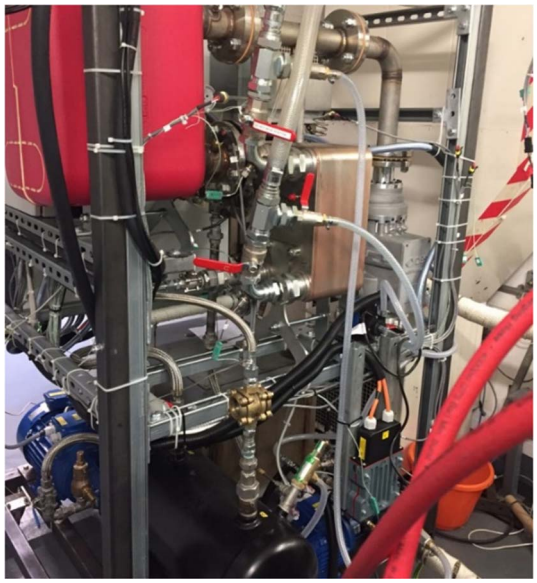

Fig. 4. The ORC skid constructed for ICE waste heat recovery testing.

Table 2
Characteristics of the heavy duty diesel engines.

Displaced Volume	7255 cc	Number of cylinders	6
Stroke	132 mm	Number of valves	4
Bore	108 mm	Maximum torque	1100 Nm @ 1400–1600 RPM
Compression Ratio	17.5:1	Maximum power	206 kW @ 2300 RPM

4.2.1. Gas-oil heat exchanger (main heat exchanger)

In the gas-oil heat exchanger (Fig. 3), heat transfer takes place between the exhaust gases of the engine and the thermal oil. It is a single heat flow, shell and tube heat exchanger manufactured by Entropea Labs.

4.2.2. Evaporator, condenser and recuperator

The evaporator, condenser and recuperator units are all counter current flow, brazed plate heat exchangers. The counter current configuration in the condenser is beneficial to ensure that saturated liquid leaves the condenser, thereby, allowing the working fluid pump to

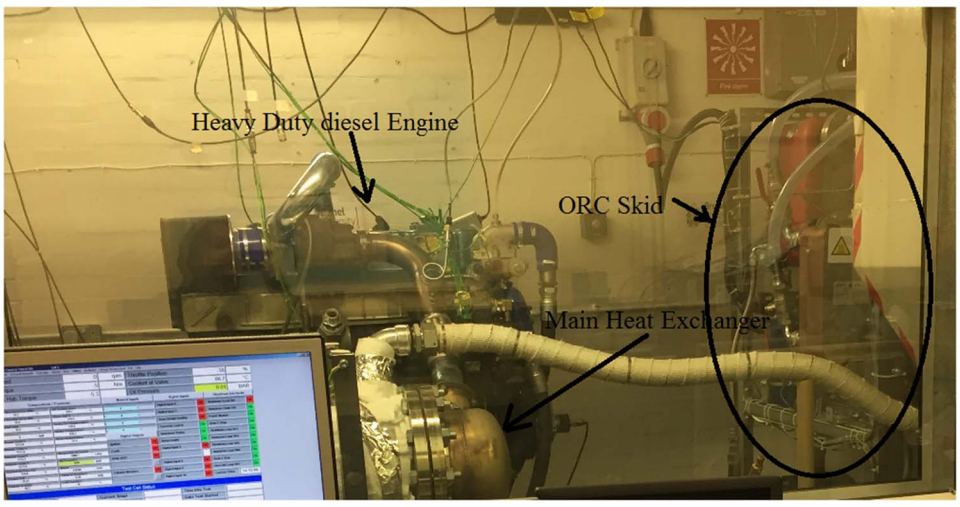

Fig. 3. Engine-ORC installation with main test components identified.

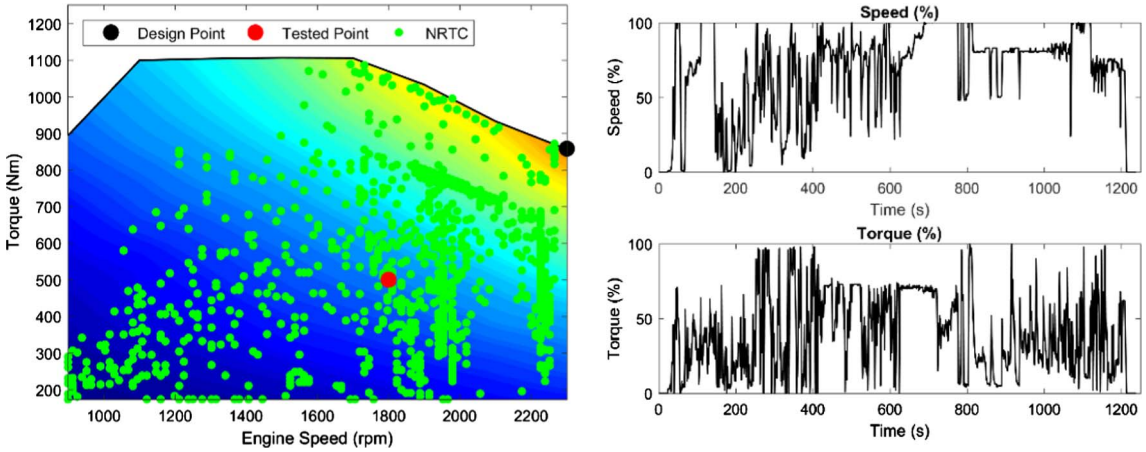

Fig. 5. (a) left: Exhaust heat diesel engine map, (b) right: The Nonroad Transient Cycle (NRTC) protocol.

Table 3
Pumps specifications.

Pump	Speed (RPM)	Flow rate (lt/min)	Maximum power (kW)
Oil pump	1400	40	1.1
Working fluid pump	1400	60	5.5

operate more efficiently. The brazing is made of copper and connections inside the heat exchangers are made of stainless steel to withstand the operating conditions of the cycle. Brazed plate heat exchangers consist of a pack of plates that are pressed together which eliminates the use of gaskets. The maximum temperature and test pressure of the heat exchangers are 225 °C and 46 bar for the evaporator, 225 °C and 40 bar for the condenser, and 225 °C and 72 bar for the recuperator. The condenser is cooled by a water loop that is controlled by a throttling valve.

4.2.3. Pumps

There are two pumps available in the test rig – one for the oil loop and the other for working fluid loop. Both pumps are of positive displacement type (gear pumps). The pumps are connected to an electrical motor with the same maximum speed. The characteristics of both pumps are listed in Table 3.

4.2.4. Turbine

The turbine was designed according to the methodology presented in Fig. 6. Firstly, the basic geometry was constructed using a mean-line model. Then, the 3D parts of the turbine were constructed as shown in Fig. 7. The turbine then was optimized through dedicated CFD investigations. Finally, the turbine was manufactured as shown in Fig. 7. The detailed design methodology is presented in previous paper by the authors [65]. Table 4 presents the main geometrical parameters of the turbine. The turbine was designed with novel back-swept blading in order to increase the tangential velocity component and hence higher power output as expressed in Eq. (5).

The radial inflow turbine was designed mainly for this application considering the exhaust gas temperature of the engine at full load as the heat source for the thermal oil loop. After extensive ORC simulations by the industrial partner, the design point operating conditions of the turbine were specified as shown in Table 5. The turbine shown in Fig. 7 was designed based on the design point conditions shown in the table. At the design point, the theoretical and CFD results showed that the turbine could produce power output of 18 kW and operate with a total

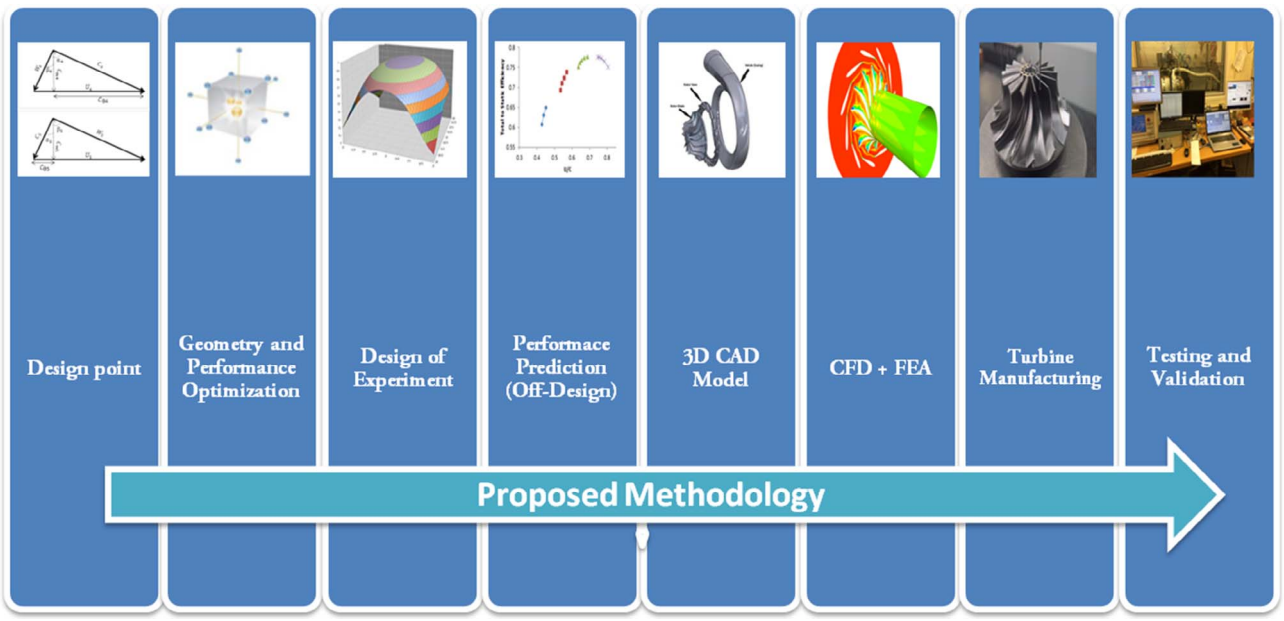

Fig. 6. The design methodology employed in the design of the radial inflow turbine.

(a) Turbo-generator

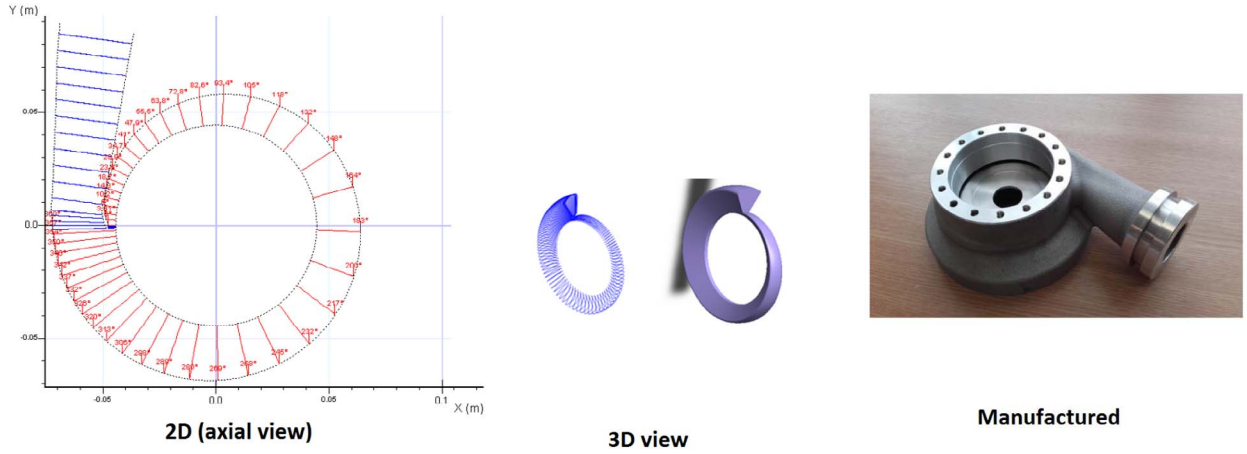

(b) Volute views (2D, left; 3D, middle and manufactured, right)

(c) Stator views (design, left and manufactured, right)

Fig. 7. Details of the radial inflow turbine.

to static efficiency of 75.2%. The maximum theoretical thermal efficiency was 9.3%.

However, due to the limitation of the dynamometer, the engine was not running at full load. In fact, the engine could only provide a torque of 450 N.m which for the maximum speed tested (1700 rpm) equated to 81 kW. Therefore, the turbine was tested at highly off-design conditions as shown in Table 5. Indeed, this could be more beneficial since the exhaust gas temperature is unstable and uncontrollable, thereby obtaining more practical results. In addition, off-design point is the frequent engine operating point, as shown in Fig. 5.

4.3. Instrumentation

The test facility is instrumented with measuring devices at inlet and

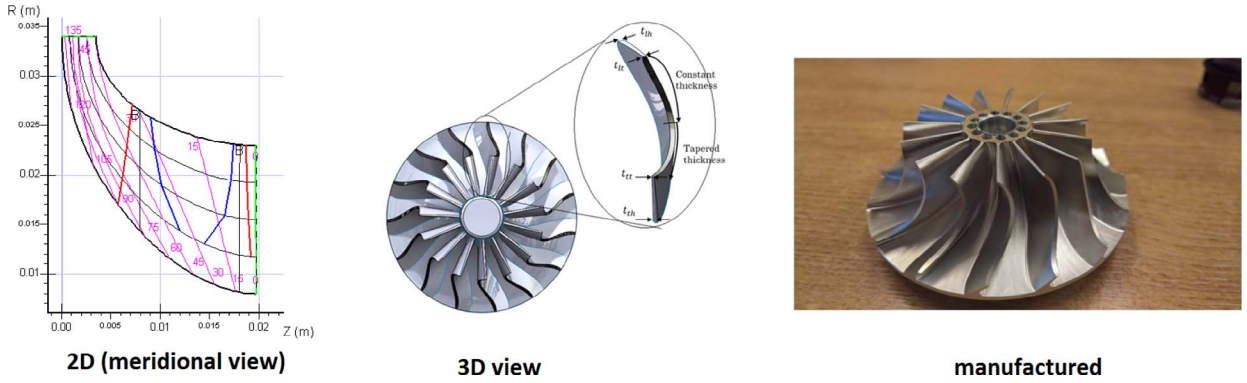

(d) Rotor views (2D, left; 3D, middle and manufactured, right)

Fig. 7. (*continued*)

Table 4
Basic geometrical data of the radial turbine.

Parameter	Unit	Design point	Off-design (Testing)
Turbine inlet total pressure	bar	13	1.8–9
Turbine inlet total temperature	K	471.5	423.15–437.5
Turbine exit static pressure	bar	1.3	1.1–1.4
Turbine inlet mass flow rate	kg/s	0.923	0.03–0.815
Rotational speed	rpm	40,000	15,000–20,000

Table 5
Design and off design conditions for the radial inflow turbine.

Parameter	Value
Stator inlet radius [mm]	44.4
Stator exit radius [mm]	35.5
Stator blade height [mm]	3.4
Rotor inlet radius [mm]	34.1
Radius exit radius (rms) [mm]	17.2
Rotor inlet blade height [mm]	3.4
Rotor exit blade height [mm]	15
Rotor inlet blade angle [deg]	54
Rotor exit blade angle [deg]	−45
Number of rotor blades [–]	15
Number of stator vanes [–]	17

Table 6
Operating range and accuracy of the measuring devices.

Measurement	Range	Accuracy
Total temperature	−40 to 1100 °C	± 1.1 °C
Total pressure	1–50 bar	± 0.25 full scale
Working fluid flow rate	0.23–1.82 m^3/h	± 3% of reading

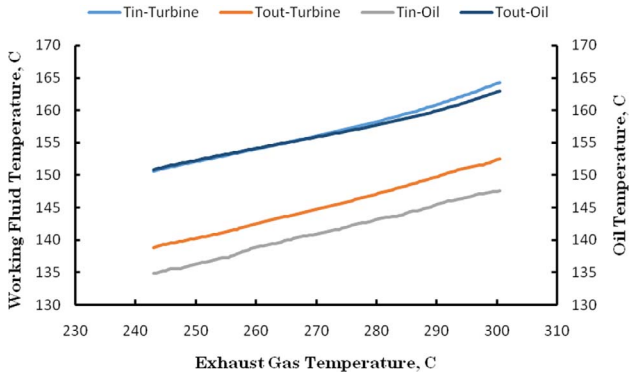

Fig. 8. Effect of heat source temperature on working fluid and oil temperature.

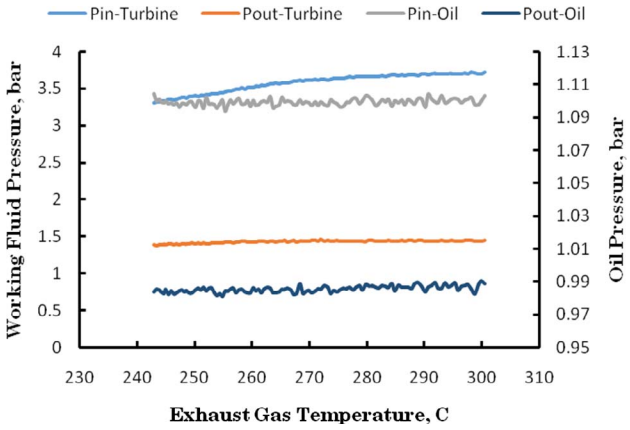

Fig. 9. Effect of heat source temperature on working fluid and oil pressures.

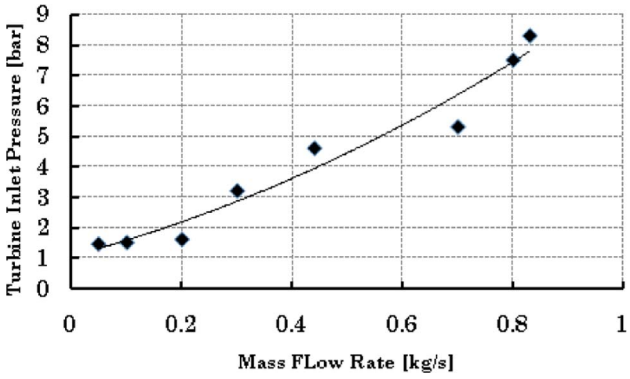

Fig. 10. Effect of working fluid mass flow rate on turbine inlet pressure.

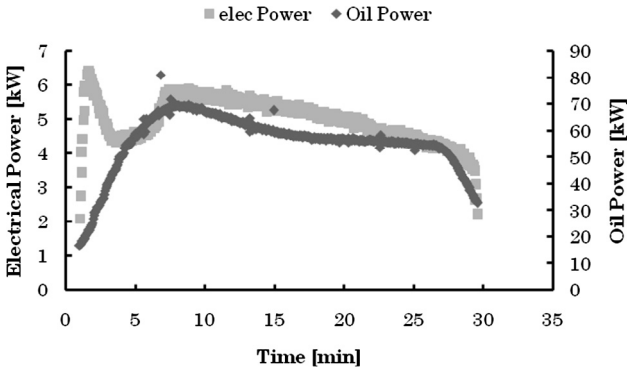

Fig. 11. Relationship between Oil Power and Electrical Power.

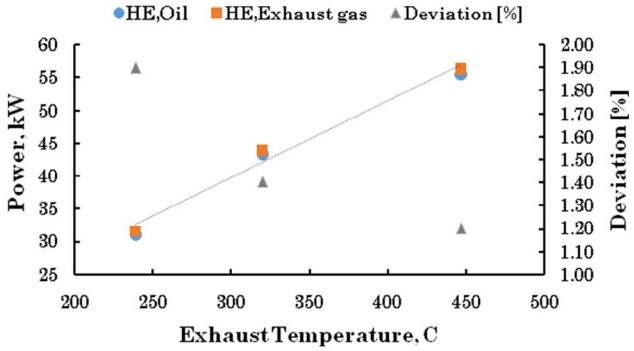

Fig. 12. Energy balance through the main heat exchanger.

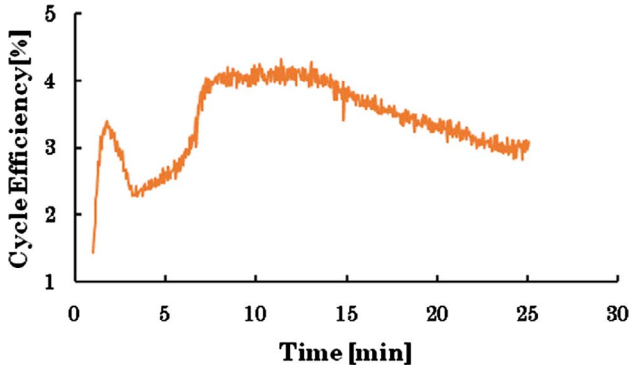

Fig. 13. Cycle efficiency evolution with time.

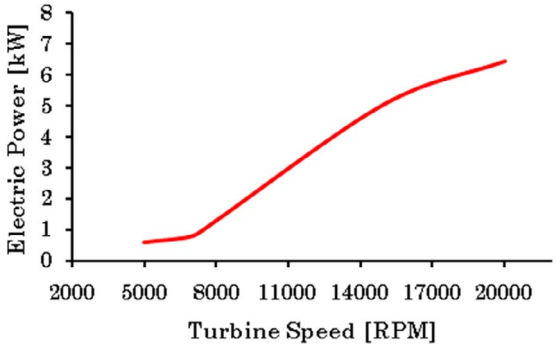

Fig. 14. Power generation with speed.

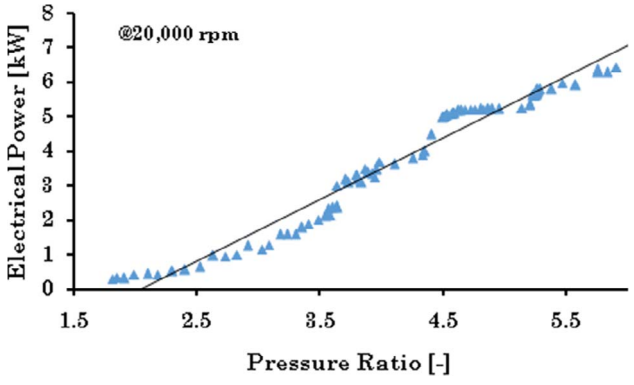

Fig. 15. Power generation with turbine pressure ratio at 20,000 rpm.

exit of the components in order to measure total pressure, total temperature and/or mass flow rate. This is aimed at evaluating ORC efficiency, turbine power and efficiency, and the generated electrical power at different operating conditions. All the thermocouples are of K

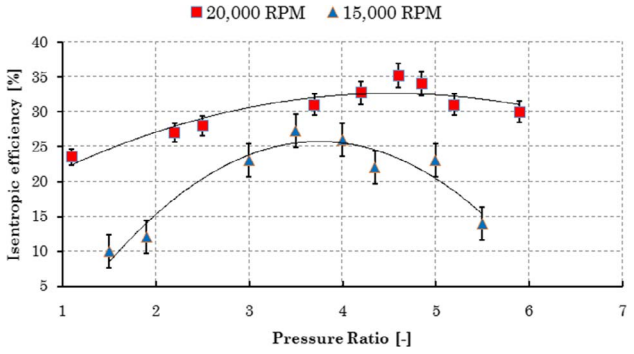

Fig. 16. Turbine isentropic efficiency at two different speeds.

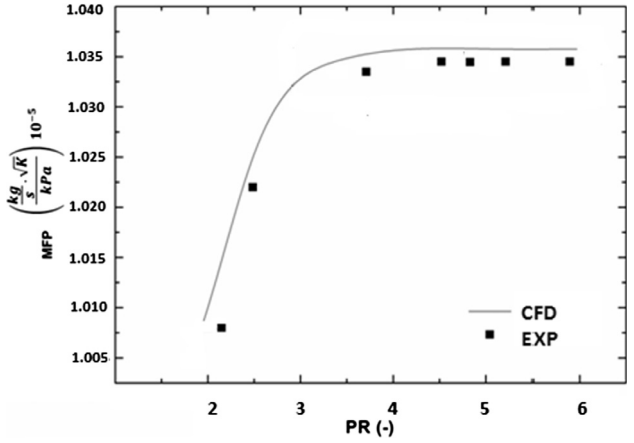

Fig. 17. Mass flow parameter vs pressure ratio.

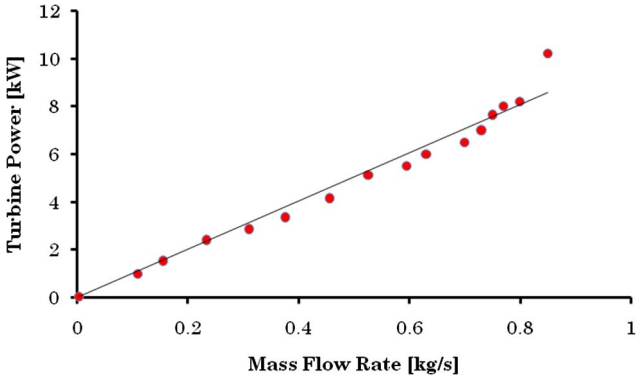

Fig. 18. Variation of power with working fluid mass flow rates.

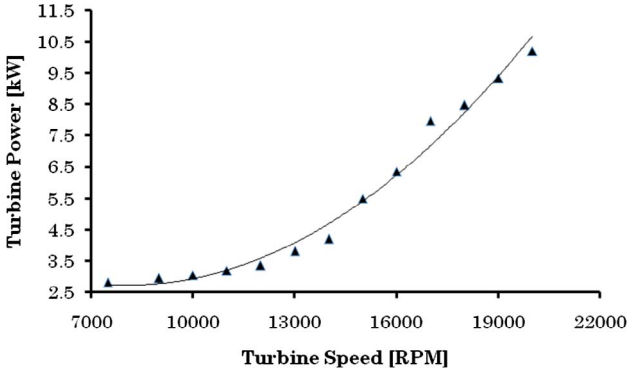

Fig. 19. Variation of power with turbine speed.

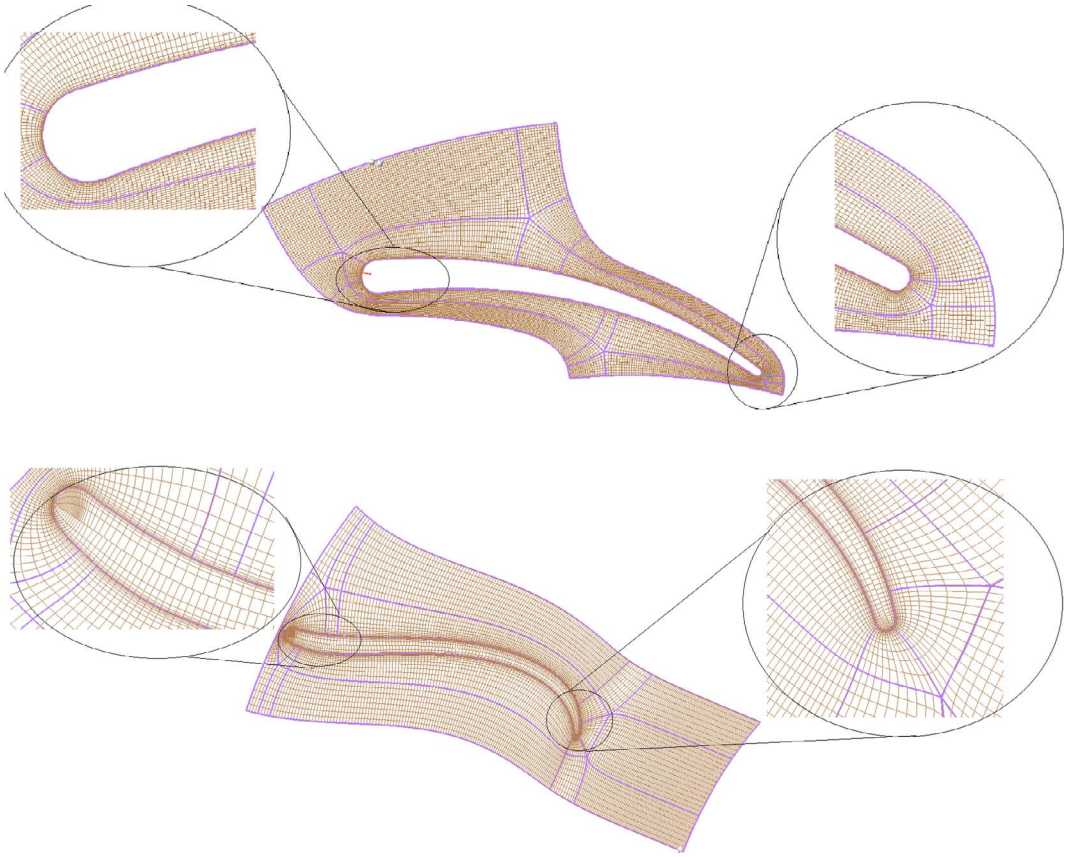

Fig. 20. Stator mesh (top) and rotor mesh (bottom).

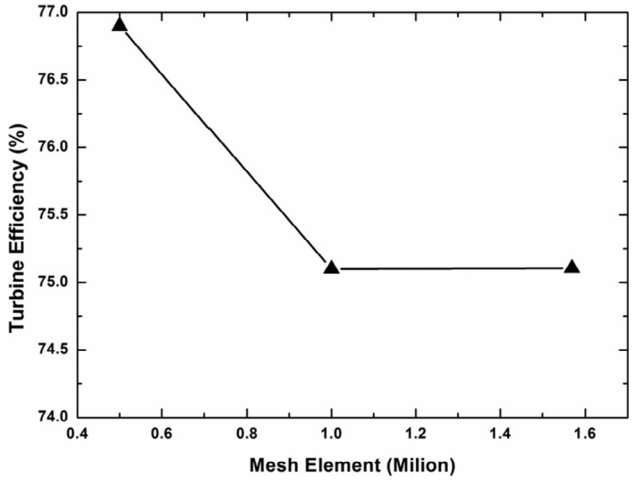

Fig. 21. Mesh dependence study.

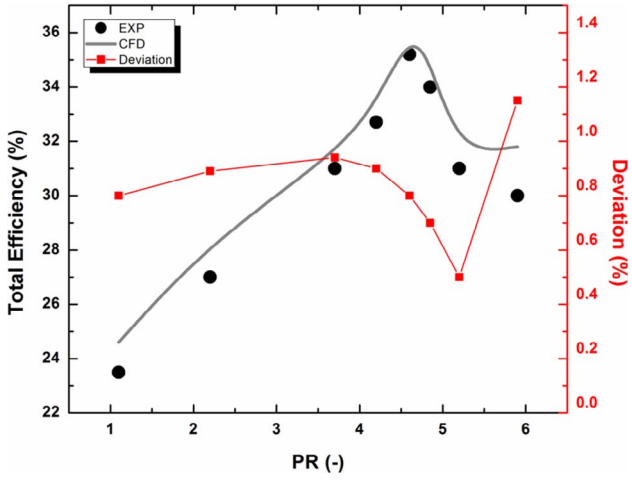

Fig. 22. Comparison of the turbine total efficiency between the experimental and CFD results.

type (Nickel Chromium/Nickel Aluminium). They are highly flexible and the sheath can be formed or bent to suit the applications required. The pressure transducers use piezo-resistive sensing technology with ASIC (Application Specific Integrated Circuit) signal conditioning in brass housing and Metri-Pack 150 or cable harness electrical connections. The mass flow rates of thermal oil and working fluid are measured using flow meters. The turbine is directly coupled to the generator and the speed can be controlled by the user. The operating range and accuracy of the measuring devices are described in Table 6.

5. Results and discussion

5.1. Overview of the results

The recording of the test data was initiated once thermal equilibrium (steady state) was achieved. Therefore, the time (x-axis) shown in latter figures in this section is the time after recording and not the time from the start of the test.

The exhaust gas temperature is the main external factor that affects cycle performance. Figs. 8 and 9 present the impact of the exhaust gas temperature on temperature and pressure of both the oil through the evaporator, and the working fluid through the turbine at constant

working fluid mass flow rate (0.33 kg/s). It is clear from Fig. 8 that the oil temperature increases at a constant rate as the exhaust gas temperature increases. Consequently, the temperature of the working fluid at the turbine inlet increases proportionately. It is also noticed that the turbine exit temperature increases proportionately as the exhaust gas temperature increases. The temperature drop between inlet and exit of the turbine is a result of the expansion process within the turbine. The maximum temperature difference of the oil between evaporator inlet and exit is 14.4 °C while it is 12.3 °C of the organic fluid between turbine inlet and exit at the maximum exhaust gas temperature. Fig. 9 presents the influence of the exhaust gas temperature on the oil and working fluid pressure. The increase of the oil pressure at inlet and exit of the main heat exchanger is negligible which indicates a steady state condition. The turbine inlet pressure increases by 0.4 bar as the exhaust gas temperature increases. On the other hand, the turbine exit pressure is almost constant during the process since the exit pressure is not directly related to the evaporator exit. As mentioned earlier, this sample of results are taken at constant working fluid mass flow rate. Fig. 10 shows that the turbine inlet pressure increases with increasing the working fluid mass flow rate. As the mass flow rate increases from 0.05 kg/s to 0.83 kg/s, the turbine inlet pressure increases from 1.45 bar to 8.3 bar.

As stated before the tests were run at 81 kW of engine power (40% of the maximum engine power). Therefore, heating of the thermal oil could not be sustained which diminished the oil power with time. Hence, the power generation in the electric generator lasts for about 30 min with a maximum power of 6.3 kW before it fell sharply in the last five minutes. Fig. 11 presents the variation of the electrical and oil power with time.

The equations presented in Table 1 were applied in order to calculate the performance for the three heat exchangers involved (gas-oil heat exchanger, evaporator and condenser) at different heat source temperatures. It is worth mentioning that the points, where two-phase flow occurs, were excluded in the analysis due to the difficulty of measuring the thermodynamic properties (i.e. enthalpies) involved at those stations. As can be seen in Fig. 12, the maximum deviation in the main heat exchanger (gas-oil heat exchanger) is 1.9% at 239 °C. The same analysis was performed on the evaporator and the condenser. The maximum errors for the two components were 3.7% and 4.1%, respectively. The above errors are relatively low and could be explained due to inaccuracies in the temperature measurements and the heat loss in the connecting pipes as these pipes were not insulated during the test.

The thermal efficiency of the cycle was investigated with time as depicted in Fig. 13. It is worth pointing out that the cycle efficiency is far below the design point value (9.3%) as the cycle was operated well within off-design conditions. For instance, the turbo-generator operated at 20,000 rpm which is far below its rated rotational speed (40,000 rpm). The cycle efficiency was in the range of 1.4–4.3%. The efficiency reached its peak after about 12 min of testing and then decreased to 2.8% due to the reduction of the electrical power in the generator (Fig. 11).

The main purpose of the ORC as a waste heat recovery system is to improve the engine performance or conversely the reduction of fuel consumption. The results reveal that the BSFC was decreased by an average value of 3% after the implementation of the ORC at these conditions (40% of the maximum engine power).

5.2. Turbo-generator characteristics

5.2.1. Electrical power

The electrical power generated by the generator is investigated at different conditions. Fig. 14 reveals the relationship between the generated power and the turbo-generator speed. It is clear that the electrical power increases linearly as the speed increases. As the speed increases from 5000 to 7000 rpm, the power increase is insignificant. The power then increases gradually from 8000 to 20,000 rpm with a maximum power of 6.3 kW at 20,000 rpm. In addition, the generated power is investigated at different turbine pressure ratios as can be seen in Fig. 15. The generated power linearly increases as the expansion ratio between turbine inlet and exit increases. It is worth mentioning that the expansion is increased by controlling the mass flow rate using the working fluid gear pump. As the mass flow rate increases, the turbine inlet pressure increases as demonstrated in Fig. 10. It is also worth noting that the results in Fig. 15 are demonstrated at constant turbo-expander speed (20,000 rpm). The maximum obtained electrical power is 6.3 kW at 5.9 pressure ratio. For the 15,000 rpm speed, the maximum electrical power achieved is 5.1 kW at 3.8 pressure ratio.

5.2.2. Turbine performance

The turbine performance is investigated at different speed and mass flow rate conditions, and at constant heat source temperature.

For the evaluation of the efficiency of the turbo-expander, the isentropic total-to-total efficiency definition is applied as shown in Eq. (3). The heat source temperature is kept constant while the mass flow is increased in order to control the pressure ratio through expander for each speed line. The turbine is directly coupled to the generator. Therefore, the turbo-generator speed can be controlled by the user. Two speed lines are selected, namely; 15,000 and 20,000 rpm. As stated, 20,000 rpm is the maximum allowable speed due to the limitation of the engine dynamometer. Each single value of pressure ratio is taken as the average value for about 3 min of testing. As can be seen in Fig. 16, both speed lines have the same trend where the efficiency increases until reaching its peak then decreases as the pressure ratio increases. This decrease is expected in radial turbines due to the choked flow at high pressure ratios as can been seen in Fig. 17. At PR ≥ 4.2, the flow becomes supersonic at the nozzle exit which results in choking condition for any further increase in the pressure ratio. In case of choking, total losses especially the incidence and frictional losses also increase. The choking condition results also in raising the flow velocity in the rotor much more than in the nozzle. The latter phenomenon results in shock waves in the radial gap between the stator exit and rotor inlet. The aforementioned problems arising from the flow choking result in lower turbine efficiency as the pressure ratio exceeds the choked value. With the 20,000 rpm speed, the efficiency increases with increasing the pressure ratio until it reaches its peak of 35.2% before it decreases to 30% at 5.9 pressure ratio. At the 15,000 rpm, the isentropic efficiency varies from 10%, reaching its peak of 27.3%, to 14% at a pressure ratio of 5.5. The cumulated measurement uncertainty is nearly constant for each speed line. For the 20,000 rpm, the uncertainty measurement is 1.5%, while it is approximately3% for the 15,000 rpm.

In addition, the turbine power is investigated at different mass flow rates and speeds. The results are presented in Figs. 18 and 19. The power of the turbine increases linearly as the mass flow increases. Increasing the mass flow rate, by adjusting the gear pump, results in a higher pressure ratio through the turbine stage. As the pressure ratio increases, the enthalpy drop increases leading to higher turbine power output. As shown in Fig. 18, the maximum obtained power is 10.2 kW at 0.85 kg/s mass flow rate. According to Eq. (4), the higher the turbine speed is, the more power is obtained. Unlike mass flow rate, turbine power increases non-linearly along with the increase in the turbine speed with a maximum value of 10.2 kW at 20,000 rpm as depicted in Fig. 19. The non-linear increasing of turbine power is justified by the term $(U_4^2 - U_5^2)$ which represents the first term of Eq. (6).

5.3. Computational fluid dynamics (CFD)

Since the tests were performed at highly off-design conditions, the turbine performance was further evaluated using the CFD results. The stator vanes and rotor blades were designed using the BladeGen tool in ANSYS and then imported to the ANSYS TurboGrid to generate the appropriate meshes, as shown in Fig. 20. In this study, an automatic

topology (ATM Optimised) was selected so that ANSYS TurboGrid could select the suitable topology for the blade passage. If the mesh quality at a certain region, such as the rotor leading edge, is poor, then the control points can be adjusted by the user to solve the problem. Fig. 21 presents the sensitivity analysis of the element number of the passage to the turbine isentropic efficiency at the design point. The passages with one million elements were selected for the current study.

Two models of boundary conditions can be applied in ANSYS CFX. The first model applies total pressure and temperature at the turbine inlet, whereas the second model is defined with the combination of mass flow rate at the inlet and static pressure at the outlet. In this study, the first model was applied because it provides the best numerical stability and convergence rates [66]. To include the effect of heat transfer, the total energy model was included in the simulation because it depicts the transport of enthalpy and considers the flow kinetic energy [67]. All solid surfaces were modelled as smooth walls using a no-slip boundary condition. The parameters of the off-design conditions shown in Table 5 were applied with the rotational speed kept 20,000 rpm. In order to define the working fluid, look-up table were built and discretised in 500×500 arrays with pressure (50–13,500 kPa) and temperature (350–500 K) as independent variables.

The results of the parametric CFD study were in good agreement with the experimental results as shown Fig. 22. The maximum deviation was 1.15% at $PR = 5.9$. For the rest of the range, the deviations were less than 1%. These insignificant deviations indicate that the CFD study is properly set, and the experimental results are reliable.

6. Conclusion

A compact ORC system was built, coupled to a heavy duty diesel engine and tested. A thermal oil loop was constructed to absorb the wasted heat in the exhaust and deliver it to the organic fluid. This helped to control the operating conditions in and out of the different ORC components; hence steady state was reached prior to testing. The intermediate oil loop was necessary to preserve the integrity of the working fluid selected but increased the system complexity and cost and resulted in lower system efficiency. Therefore, its choice is dependent on working fluid selection and ultimate application.

In addition, a radial inflow turbine was designed specifically for the current application considering the cycle conditions and the thermodynamic properties of the organic fluid. The overall cycle and the turbogenerator performance were investigated.

The results revealed that the maximum generated power was 6.3 kW at 20,000 rpm at 40% engine power. The operating conditions were a substantially off-design condition, at which the peak efficiency of the radial turbine was 35.2% at 20,000 rpm. In addition, the maximum thermal efficiency of the cycle was 4.3%. The results also revealed that the coupled engine-ORC system improved the engine power and the BSFC by 3% at the tested engine point. For more assurance, the experimental results of the turbine were compared with the CFD results due to the highly off-design conditions. The numerical and experimental results were in good agreement with a maximum deviation of 1.15%.

The results of the current study were encouraging for further investigation including design conditions as well as transient driving cycles.

Acknowledgements

The authors would like to acknowledge the financial support of Innovate UK to this project (ref. TS/M012220/1). The authors would like also to thank Dr. Konstantinos Tsamos and Dr. Giuseppe Bianchi from Brunel University London for their fruitful ideas on the experimental part of this work.

References

[1] NRC. Review of the 21st century truck partnership. Washington (D.C.): The National Academies Press; 2008.
[2] Zhang XX, Zeng K, He MG. New technology of thermodynamic cycle for waste heat recovery of vehicle gasoline engine. 2009 Asia-Pacific power and energy engineering conference. 2009. p. 1–6.
[3] Hountalas DT, Katsanos C, Lamaris VT. Recovering energy from the diesel engine exhaust using mechanical and electrical turbocompounding. SAE technical paper, no. 724; 2007. p. 776–90.
[4] Zhao R, Li W, Zhuge W, Zhang Y, Yin Y. Numerical study on steam injection in a turbocompound diesel engine for waste heat recovery. Appl Energy 2017;185(Part 1):506–18.
[5] Karvountzis-Kontakiotis A, et al. Effect of an ORC waste heat recovery system on diesel engine fuel economy for off-highway vehicles; 2017.
[6] Stobart R, Milner D. The potential for thermo-electric regeneration of energy in vehicles. 2009 SAE international, no. 2009-01-13; 2009.
[7] Stobart RK, Wijewardane A, Allen C. The potential for thermo-electric devices in passenger vehicle applications. SAE technical paper 2010-01-0833; 2010.
[8] Wang Y, Dai C, Wang S. Theoretical analysis of a thermoelectric generator using exhaust gas of vehicles as heat source. Appl Energy 2013;112(C):1171–80.
[9] Karvountzis-Kontakiotis A, Alshammari F, Pesiridis A, Franchetti B, Pesmazoglou I, Tocci L. Variable geometry turbine design for off-highway vehicle organic Rankine cycle waste heat recovery. THIESEL 2016 conference on thermo-and fluid dynamic processes in direct injection engines, Valencia, Spain. 2016.
[10] Still WJ. International combustion engine. England Patnet 1230617; 1917.
[11] Legros A, Guillaume L, Lemort V, Diny M, Bell I, Quoilin S. Investigation on a scroll expander for waste heat recovery on internal combustion engines. Int Conf Compressors Syst 2013;1:10.
[12] Patel E, Doyle P. Compounding the truck diesel engine with an organic Rankine-cycle system. SAE tech pap 760343; 1976.
[13] Newton PJ, Martinez-botas RF, Robertson Miles C, Costall Aaron W. Transient duty cycle analysis for mobile organic Rankine cycle applications. 3rd International seminar on ORC power systems. 2015.
[14] Morgan R, Dong G, Panesar A, Heikal M. A comparative study between a Rankine cycle and a novel intra-cycle based waste heat recovery concepts applied to an internal combustion engine. Appl Energy 2016;174(Supp. C):108–17.
[15] Karvountzis-Kontakiotis A, Alshammari F, Pesiridis A. Design of radial turbine expanders for organic Rankine cycle, waste heat recovery in high efficiency, off-highway vehicles. 3rd Annual engine ORC consortium workshop, Queens University Belfast, UK, 14–16 September 2016. 2016.
[16] Alshammari F, Karvountzis-Kontakiotis A, Pesiridis A. Radial turbine expander design for organic Rankine cycle, waste heat recovery in high efficiency, off-highway vehicles. 3rd Biennial international conference on powertrain modelling and control (PMC 2016), Loughborough, UK. 2016.
[17] Guillaume L, Legros A, Desideri A, Lemort V. Performance of a radial-inflow turbine integrated in an ORC system and designed for a WHR on truck application: an experimental comparison between R245fa and R1233zd. Appl Energy 2017;186:408–22.
[18] Arunachalam PN, Shen M, Tuner M, Tunestal P, Thern M. Waste heat recovery from multiple heat sources in a HD truck diesel engine using a Rankine cycle – a theoretical evaluation. SAE 2012 international powertrains, fuels & lubricants meeting. 2012.
[19] Endo T, et al. Study on maximizing exergy in automotive engines. SAE tech pap ser; 2007.
[20] Koppauer H, Kemmetmüller W, Kugi A. Modeling and optimal steady-state operating points of an ORC waste heat recovery system for diesel engines. Appl Energy 2017;206(Suppl. C):329–45.
[21] Song J, Gu C. Performance analysis of a dual-loop organic Rankine cycle (ORC) system with wet steam expansion for engine waste heat recovery Suppl. C Appl Energy 2015;156:280–9.
[22] Sprouse C, Depcik C. Review of organic Rankine cycles for internal combustion engine exhaust waste heat recovery. Appl Therm Eng 2013;51(1–2):711–22.
[23] Fiaschi D, Manfrida G, Maraschiello F. Thermo-fluid dynamics preliminary design of turbo-expanders for ORC cycles. Appl Energy 2012;97:601–8.
[24] Ziviani D, Beyene A, Venturini M. Advances and challenges in ORC systems modeling for low, grade thermal energy recovery. Appl Energy 2014;121(Suppl. C):79–95.
[25] Lu Y, Wang Y, Wang L, Yuan Y, Liu Z, Roskilly AP. Experimental investigation of a scroll expander for power generation part of a resorption cogeneration Suppl. C Energy Procedia 2015;75:1027–32.
[26] Erba M, Biyikoglu A. Design of low temperature organic Rankine cycle and turbine. 4th Int conf power eng energy electr drives, no. May. 2013. p. 1065–70.
[27] Rahbar K, Mahmoud S, Al-Dadah RK. Mean-line modeling and CFD analysis of a miniature radial turbine for distributed power generation systems. Int J Low-Carbon Technol 2014:1–12.
[28] Bao J, Zhao L. A review of working fluid and expander selections for organic Rankine cycle. Renew Sustain Energy Rev 2013;24:325–42.
[29] Qiu G, Liu H, Riffat S. Expanders for micro-CHP systems with organic Rankine cycle. Appl Therm Eng 2011;31(16):3301–7.
[30] Stobart R, Weerasinghe R. Heat recovery and bottoming cycles for SI and CI engines – a perspective. SAE techinical pap 2006-01-0662, vol. 2006, no. 724; 2006.
[31] Saadatfar B, Fakhrai R, Fransson T. Waste heat recovery Organic Rankine cycles in sustainable energy conversion: a state-of-the-art review. J MacroTrends Energy Sustain 2013;1(1):161–88.

[32] Rosset K, Mounier V, Eliott Guenat OP, Schiffmann J. Potential of small-scale turbomachinery for waste heat recovery on automotive internal combustion engines. 3rd International seminar on ORC power systems, October 12–14, 2015, Brussels, Belgium. 2015.
[33] Liu Z, et al. Modelling and optimisation on scroll expander for waste heat recovery organic Rankine cycle. Energy Procedia 2015;75:1603–8.
[34] Qiu K, Thorsteinson E. An organic Rankine cycle system for solar thermal power applications. International conference on renewable energy research and application (ICRERA), Milwaukee, USA. 2014.
[35] Chambers T, Raush J, Russo B. Installation and operation of parabolic trough organic Rankine cycle solar thermal power plant in South Louisiana Suppl. C Energy Procedia 2014;49:1107–16.
[36] Quoilin S, Orosz M, Hemond H, Lemort V. Performance and design optimization of a low-cost solar organic Rankine cycle for remote power generation. Sol Energy 2011;85(5):955–66.
[37] Wang XD, Zhao L, Wang JL, Zhang WZ, Zhao XZ, Wu W. Performance evaluation of a low-temperature solar Rankine cycle system utilizing R245fa. Sol Energy 2010;84(3):353–64.
[38] Petrollese M, Cocco D, Cau G. Small-scale CSP plant coupled with an ORC system for providing dispatchable power: the Ottana Solar Facility. Energy Procedia 2017;129(Suppl. C):708–15.
[39] Kolasinski P, Blasiak P, Rak J. Experimental investigation on multi-vane expander operating conditions in domestic CHP ORC system. Energy Procedia 2017;129(Suppl. C):323–30.
[40] Landelle A, Tauveron N, Haberschill P, Revellin R, Colasson S. Organic Rankine cycle design and performance comparison based on experimental database. Appl Energy 2017;204:1172–87.
[41] Liu H, Qiu G, Shao Y, Daminabo F, Riffat SB. Preliminary experimental investigations of a biomass-fired micro-scale CHP with organic Rankine cycle†. Int J Low-Carbon Technol 2010;5(2):81–7.
[42] Qiu G, Shao Y, Li J, Liu H, Riffat SB. Experimental investigation of a biomass-fired ORC-based micro-CHP for domestic applications. Fuel 2012;96:374–82.
[43] Ancona MA, et al. A micro-ORC energy system: preliminary performance and test bench development Suppl. C Energy Procedia 2016;101:814–21.
[44] Zywica G, Kaczmarczyk TZ, Ihnatowicz E, Turzynski T. Experimental investigation of the domestic CHP ORC system in transient operating conditions. Energy Procedia 2017;129(Suppl. C):637–43.
[45] Bliem CJ, Mines GL. Initial results for supercritical cycle experiments using pure and mixed-hydrocarbon working fluids. Trans – Geotherm Resour Council 1984;8:27–32.
[46] Li M, et al. Construction and preliminary test of a low-temperature regenerative Organic Rankine Cycle (ORC) using R123. Renew Energy 2013;57(Suppl. C):216–22.
[47] Tang H, Wu H, Wang X, Xing Z. Performance study of a twin-screw expander used in a geothermal organic Rankine cycle power generator. Energy 2015;90(Part 1):631–42.
[48] Klonowicz P, Borsukiewicz-Gozdur A, Hanausek P, Kryłłowicz W, Brüggemann D. Design and performance measurements of an organic vapour turbine. Appl Therm Eng 2014;63(1):297–303.
[49] Zhang HG, Wang EH, Fan BY. A performance analysis of a novel system of a dual loop bottoming organic Rankine cycle (ORC) with a light-duty diesel engine. Appl Energy 2013;102(Suppl. C):1504–13.
[50] Furukawa T, Nakamura M, Machida K, Shimokawa K. A study of the Rankine cycle generating system for heavy duty HV trucks. SAE tech pap; 2014.
[51] Wang E, Yu Z, Zhang H, Yang F. A regenerative supercritical-subcritical dual-loop organic Rankine cycle system for energy recovery from the waste heat of internal combustion engines. Appl Energy 2017;190(Suppl. C):574–90.
[52] Shao L, Ma X, Wei X, Hou Z, Meng X. Design and experimental study of a small-sized organic Rankine cycle system under various cooling conditions. Energy 2017;130(Suppl. C):236–45.
[53] Pang K-C, et al. Experimental study on organic Rankine cycle utilizing R245fa, R123 and their mixtures to investigate the maximum power generation from low-grade heat. Energy 2017;133(Suppl. C):636–51.
[54] Yang F, Cho H, Zhang H, Zhang J. Thermoeconomic multi-objective optimization of a dual loop organic Rankine cycle (ORC) for CNG engine waste heat recovery. Appl Energy 2017;205(Suppl. C):1100–18.
[55] Sellers C. Field operation of a 125kW ORC with ship engine jacket water. Energy Procedia 2017;129(Suppl. C):495–502.
[56] Glensvig M, et al. Testing of a long haul demonstrator vehicle with a waste heat recovery system on public road. SAE 2016 commercial vehicle engineering congress. 2016.
[57] Endo T, et al. Study on maximizing exergy in automotive engines. SAE world congress & exhibition. Michigan: Detroit; 2007.
[58] Ibaraki S, Endo T, Kojima Y, Takahashi T, Baba T, Kawajiri S. Research of a Rankine Cycle on-board heat waste heat recovery system. J Soc Automot Eng Japan 2006.
[59] MAN. Waste Heat Recovery System (WHRS) reduction of fuel consumption, emission and EEDI; 2012.
[60] Roy JP, Mishra MK, Misra A. Performance analysis of an Organic Rankine Cycle with superheating under different heat source temperature conditions. Appl Energy 2011;88(9):2995–3004.
[61] Franchetti B, Pesiridis A, Pesmazoglou I, Sciubba E, Tocci L. Thermodynamic and technical criteria for the optimal selection of the working fluid in a mini-ORC. ECOS 2016 – the 29th international conference on efficiency, cost, optimization, simulation and environmental empact of energy systems, June 19–23, 2016, Portorož, Slovenia. 2016.
[62] 3M Science Applied to Life. Organic fluids. [Online]. Available: < https://www.3m.com/ > .
[63] Lemmon E, Huber M, McLinden M. NIST standard reference database 23: reference fluid thermodynamic and transport properties-REFPROP, version 9.0. Gaithersburg, Maryland (USA): National Institute of Standards and Technology, Standard Reference Data Program; 2010.
[64] Moustapha H, Zelesky MF, Baines NC, Japikse D. Axial and radial turbines. 1st ed. White River Junction: Concepts NREC; 2003.
[65] Alshammari F, Karvountzis-Kontakiotis A, Pesiridis A, Minton T. Radial expander design for an engine organic Rankine cycle waste heat recovery system. Energy Procedia Sep. 2017;129:285–92.
[66] Simpson AT, Spence SW, Watterson JK. A comparison of the flow structures and losses within vaned and vaneless stators for radial turbines. J Turbomach 2009;131(3):31010–5.
[67] ANSYS Inc. ANSYS CFX-solver theory guide, release 15.0; 2015.